scientific reports

Check for updates

OPEN

Heterozygous interferon signaling deficient mice as animal models for Chikungunya virus infection in the heart

Shazeed-Ul Karim[1], Farzana Nazneen[1], Prince M. D. Denyoh[1], David S. Bai[2], Damian G. Romero[3,4,5,6] & Fengwei Bai[1]✉

Although chikungunya virus (CHIKV)-caused cardiovascular diseases are frequently reported in clinics, the underlying mechanisms are poorly understood, which is primarily due to a lack of animal models. In this study, we report that CHIKV infection in homozygous interferon α/β receptor-deficient (*ifnar1*$^{-/-}$) and interferon α/β/γ receptor-deficient (*ifnag*$^{-/-}$) mice resulted in high viral loads in the hearts as early as day (D) 1 post-infection (p.i.) but with 100% mortality within three days p.i. In contrast, the heterozygous *ifnar1*$^{+/-}$and *ifnag*$^{+/-}$ mice survived CHIKV infection and bore higher viral burdens in the heart tissues than the wild-type (WT) controls. Immunohistochemistry and flow cytometry revealed that more leukocytes, particularly neutrophils, infiltrated the heart of *ifnag*$^{+/-}$ and *ifnar1*$^{+/-}$ mice than WT mice. In addition, the Hematoxylin and Eosin staining analysis showed that CHIKV infection caused vasculitis in the left ventricles on D5 p.i. in both heterozygous groups and the vacuole formation and pyknosis in *ifnar1*$^{+/-}$ mice. Moreover, CHIKV infection may also lead to cardiac fibrosis, as indicated by the upregulation of the expression of the Connective Tissue Growth Factor gene in the hearts of *ifnar1*$^{+/-}$ mice. In summary, our data suggest that the heterozygous *ifnar1*$^{+/-}$ and *ifnag*$^{+/-}$ mice are invaluable for studying pathogenesis and testing therapeutic interventions for CHIKV-caused cardiac diseases.

Keywords Chikungunya virus, Interferon signaling deficient, Myocarditis, Heart, Mice

Chikungunya virus (CHIKV), a single-stranded, positive-sense RNA alphavirus in the family of *Togaviridae*, is transmitted to humans through bites by infected female *Aedes (A.)* mosquitoes, specifically *A. aegypti* and *A. albopictus*[1]. CHIKV was first isolated from a febrile patient during an outbreak in the southern province of Tanzania (formerly Tanganyika) in 1952[1,2]. From 2004 to 2011, 1.4 to 6.5 million CHIKV cases were confirmed in nearly 40 countries in Africa, Asia, and Europe[3]. Since 2014, CHIKV cases have been reported among U.S. travelers with local transmission in Florida, Texas, and Puerto Rico, and approximately 580,000 cases were reported in the Americas[4]. In the year 2022, around 270 thousand cases of CHIKV in various regions across America were reported to the Pan American Health Organization (PAHO), more than double the average annual number of cases reported between 2018 and 2021[5,6]. Although native to warm, tropical regions of Asia, *A. albopictus* has successfully adapted to cooler climates, including North America. According to the Centers for Disease Control and Prevention (CDC), *A. albopictus* now circulates in 866 counties of 26 states in the U.S., and there are large numbers of travel-related cases[7], indicating a potential epidemic risk of CHIKV in the U.S. In addition, modeling studies suggest that CHIKV infections could spread to the U.S., Canada, and Europe by 2050 due to climate change[25,26].

After an infected mosquito bite, CHIKV initially replicates in human epithelial, endothelial, and fibroblast cells at the entry site, spreads through the lymphatic system into the bloodstream, and reaches various organs, including the heart[8–10]. Although the typical clinical symptoms of CHIKV infection in humans include high fever, headache, maculopapular rashes, myalgia, edema of the extremities, and gastrointestinal complaints[11], it

[1]Cell and Molecular Biology Program, School of Biological, Environmental, and Earth Sciences, The University of Southern Mississippi, 118 College Drive # 5018, Hattiesburg, MS 39406, USA. [2]Oak Grove High School, Hattiesburg, MS 39402, USA. [3]Department of Pharmacology and Toxicology, University of Mississippi Medical Center, Jackson, MS 39216, USA. [4]Mississippi Center of Excellence in Perinatal Research, Jackson, MS 39216, USA. [5]Women's Health Research Center, Jackson, MS 39216, USA. [6]Cardiovascular-Renal Research Center, University of Mississippi Medical Center, Jackson, MS 39216, USA. ✉email: fengwei.bai@usm.edu

has been reported that 54.2% of CHIKV cases have manifested the symptoms of cardiovascular diseases (CVD) across multiple regions, including the USA, France, Sri Lanka, Malaysia, Colombia, and India[1]. Studies showed various cardiovascular events associated with CHIKV infection in humans, including hypotension, shock, circulatory collapse, arrhythmias, myocarditis, dilated cardiomyopathy, and heart failure[12,13]. Surprisingly, reports indicate that even some healthy individuals, including infants and children, have died from acute cardiac arrest, cardiorespiratory failure, and cardiac decomposition following CHIKV infection[14–16]. Postmortem analyses of patients diagnosed with idiopathic dilated cardiomyopathy showed viral infiltration of myocytes in 66% of cases[1]. The most prevalent CVD complication of CHIKV infection, which is found across nearly all age groups, is myocarditis, which results when the virus directly infects the cardiac tissue and causes cardiac injury[2,17,18]. While some of the CVD manifestations may be due to the body's immune responses to the infection, including the effects of cytokines and inflammation, other symptoms result from the direct viral invasion of the cardiac tissues[2,18–20]. All of the known cellular receptors for CHIKV, including Prohibitin (PHB), Matrix Remodeling Associated 8 (MXRA8), and Cluster of Differentiation (CD)-147, have been found on the surface of human cardiomyocytes[20]. Additionally, the CHIKV viral antigen is found in the heart tissues, and a higher CHIKV viral titer has been linked to increased cardiac damage[21–24].

Despite the critical clinical evidence, the mechanism by which CHIKV infection causes CVD remains poorly understood, mainly due to a lack of suitable animal models. In this study, we report that CHIKV infects the heart of heterozygous mice deficient in type I and II interferon receptors and manifests, at least in part, some clinical symptoms, such as cardiac tissue damage, immune cell infiltration, and fibrosis. These animal models will be invaluable in deepening our understanding of the mechanisms of CHIKV-caused heart diseases and in facilitating the development of targeted therapies.

Results

Young immunocompetent C57BL/6 mice are relatively susceptible to CHIKV infection in the heart

Previous studies have suggested that adult immunocompetent wild-type (WT) C57BL/6 mice are relatively resistant to CHIKV infection[27]. It was also observed that mice aged less than 12 days developed severe disease after CHIKV infection, resulting in deaths within 12 days post-infection (p.i.), while those older than 12 weeks exhibited a survival rate of 100%[27]. A recent study reported that CHIKV infection resulted in severe diseases in 10-12-day-old C57BL/6 mice and mortality within D7 p.i[28]. Studies assessed viral presence in various organs except for the heart and found CHIKV was present in muscle, joints, skin, brain, liver, and serum, resembling the organ involvement seen in human neonates and infants under one year old infected by CHIKV[27,29]. To examine the viral infection in the heart, we inoculated C57BL/6 mice of different age groups, ranging from 1 week (W) to 16 weeks old, with 1×10^5 plaque-forming units (PFU) of CHIKV via the footpad. The mice were sacrificed on the day (D) 1 post-infection (p.i.) to collect the heart (Fig. 1A). The CHIKV RNA was quantified by the RT-qPCR targeting the *CHIKV E1* gene, showing that the amounts of viral RNA in the heart were in an age-dependent manner with the most viral RNA presented in 1-week old mice, while it was not detectable in the heart of 8 or 16-week-old mice (Fig. 1B). Subsequently we investigated the viral presence in the heart and spleen of 3-week-old mice on different days p.i. The RT-qPCR results indicated that CHIKV RNA was present in the heart and spleen on D1 p.i., and then rapidly cleared out from these tissues (Fig. 1C and D). In summary, these results suggest that CHIKV infects the heart of young WT mice, and the viral replication may be dramatically inhibited by the host immune system, especially innate immunity.

Type I and II interferon signaling is critical to controlling CHIKV infection in the heart

CHIKV infection induces robust production of type I interferons (IFN-α/β), proinflammatory cytokines, and chemokines[30–32], and IFNα/β plays a critical role in limiting CHIKV replication at the early stage of the infection in both humans and mouse models[27]. Since CHIKV only causes a low and transient infection in the heart of young immunocompetent mice, which are not ideal for studying CHIKV-caused heart diseases, we hypothesized that mice deficient in interferon signaling might be more susceptible to the viral infection in the heart. To test this, we used interferon α/β receptor-deficient homozygous (*ifnar1*$^{-/-}$) and heterozygous (*ifnar1*$^{+/-}$) mice, as well as interferon α/β/γ receptor-deficient homozygous (*ifnag*$^{-/-}$) and heterozygous (*ifnag*$^{+/-}$) mice to assess the CHIKV infection in the heart. Three-week-old mice were infected with CHIKV, as mentioned above, and the hearts were collected on D1 p.i. with or without cardiac perfusion. The homozygous knockout (*ifnag*$^{-/-}$ and *ifnar1*$^{-/-}$) mice exhibited the highest burden in the heart compared to the heterozygous groups and WT mice under both perfused and non-perfused conditions, as determined by the RT-qPCR (Fig. 2A and D). As expected, non-perfused hearts showed slightly higher levels of viral RNA than their perfused counterparts, indicating that CHIKV was present in the blood vessels of the hearts, which was also indicated by measuring viral RNA in the blood (Fig. 2E). To confirm the RT-qPCR results, we performed a plaque-forming assay on these perfused heart samples, and consistently, the results suggest that *ifnag*$^{-/-}$ and *ifnar1*$^{-/-}$ mice were mostly susceptible to CHIKV infection in the heart, with approximately 60,000 and 25,000-fold higher than WT mice, respectively (Fig. 2B). Although the CHIKV loads in the heart of *ifnar1*$^{+/-}$ mice were lower than the homozygous knockout mice, they were 19-fold higher in the perfused heart (Fig. 2A) by RT-qPCR and 2.7-fold higher in the plaque-forming assay (Fig. 2B), and 4-fold higher in the non-perfused hearts by RT-qPCR (Fig. 2D) than the WT controls. Interestingly, the viral loads in the heart of *ifnag*$^{+/-}$ mice were similar to those of WT mice, indicating the viruses may be cleared faster from the heart of these animals than *ifnar1*$^{+/-}$ mice. RT-qPCR analysis of *Ifn-α* showed that *ifnag*$^{+/-}$ mice exhibited a trend of higher expression than *ifnar1*$^{+/-}$ mice (Fig. 2F), which likely contributes to the higher viral burden in *ifnar1*$^{+/-}$ mice. Since *ifnag*$^{-/-}$ mice were most susceptible to CHIKV infection in the hearts among all the tested mouse groups, we performed an immunohistochemistry study to evaluate the viral presence in the different parts of the heart, including the aorta, left atrium, right atrium, right ventricle and left ventricle

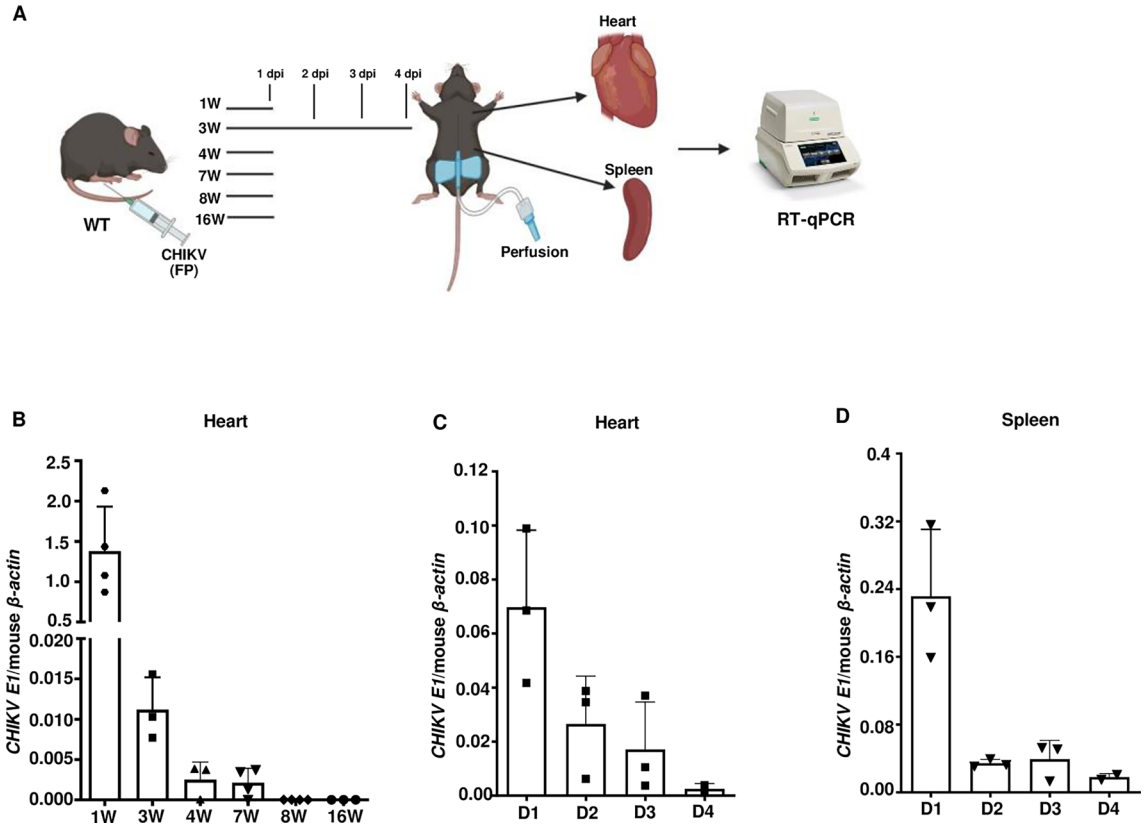

Fig. 1. Young immunocompetent WT mice are relatively susceptible to CHIKV infection in the heart. (**A**) Schematic representation of the experimental design of WT mice aged 1 to 16 weeks (W) were infected with the same viral dose (1×10^5 PFU) via footpad (FP) inoculation (Created in BioRender. BAI, F. (2025) https://BioRender.com/c59p712). Hearts were collected from the 1 W ($n = 4$), 3 W ($n = 3$), 4 W ($n = 3$), 7 W ($n = 4$), 8 W ($n = 4$), and 16 W ($n = 3$) groups on the day (D) 1 p.i. Both heart and spleen were collected from the 3 W group on D1 ($n = 3$), D2 ($n = 3$), D3 ($n = 3$), and D4 ($n = 2$) p.i. to detect CHIKV RNA by RT-qPCR. (**B**) RT-qPCR results of *CHIKV E1* expression in the hearts of the mice of different ages on D1 p.i. (**C**) RT-qPCR results of *CHIKV E1* expression in the hearts of 3 W-old mice on D1 to D4 p.i. (**D**) RT-qPCR results of *CHIKV E1* expression in the spleens of 3 W-old mice on D1 to D4 p.i.

(Fig. 2G and H). The confocal microscopy images revealed that CHIKV antigens were present in all the heart sections, with the brightest signals from the left atrium, followed by the left ventricle and aorta (Fig. 2I). These results are partially consistent with another study that evaluated the top and bottom parts of the heart separately following intravenous CHIKV infection in C57BL/6 mice and they found the top parts, which are rich in blood vessels, including the atrium and aorta, had greater susceptibility to CHIKV than the lower parts of the heart[32]. These observations led us to focus on the left atrium, left ventricle, and aorta in the following investigations.

Heterozygous IFN signaling-deficient mice are susceptible to CHIKV infection in the heart and survive the infection

To study the survival of these interferon receptor knockout mice, 3-week-old WT, *ifnar1*$^{-/-}$, *ifnar1*$^{+/-}$, *ifnag*$^{-/-}$, and *ifnag*$^{+/-}$ mice were infected with 1×10^5 PFU of CHIKV via footpad inoculation and monitored daily for 21 days. All *ifnar1*$^{-/-}$ ($n = 15$) and *ifnag*$^{-/-}$ ($n = 10$) mice died between D2 (88%) and 3 p.i. (12%); on the contrary, all *ifnar1*$^{+/-}$ ($n = 13$), *ifnag*$^{+/-}$($n = 11$), and WT ($n = 17$) mice survived by the end of the experiment without showing any disease symptoms (Fig. 3A and B). The survival results are consistent with the viral detection experiments in which the viral loads in the blood and the heart of *ifnar1*$^{-/-}$ and *ifnag*$^{-/-}$ mice were much higher than those of *ifnar1*$^{+/-}$, *ifnag*$^{+/-}$, and WT mice (Fig. 2A-E). Since death occurred within 3 days p.i. to the CHIKV-infected homozygous mice (*ifnag*$^{-/-}$ and *ifnar1*$^{-/-}$), it may hinder the use of these animals to study the disease mechanisms and test if a drug candidate could inhibit the virus-caused CVD or facilitate the disease recovery. We then investigated CHIKV infection in the hearts of the heterozygous *ifnar1*$^{+/-}$ and *ifnag*$^{+/-}$ mice. The animals were infected as above, and the hearts were collected after perfusion daily for five days p.i.. Notably, both heterozygous groups exhibited the highest viral presence on D1, followed by a rapid decline from D2 to D4, and became undetectable on D5 p.i. (Fig. 3C and D). The confocal microscopy study further confirmed that CHIKV antigens were readily detectable on D1 p.i. in the aorta, left atrium, and left ventricle of *ifnar1*$^{+/-}$ and *ifnag*$^{+/-}$ mice as well as WT, albeit the signal was relatively low in WT mice (Fig. 3E). These results align with a previous study in which CHIKV was detected in the heart of WT mice as early as 12 h p.i., peaking between D1

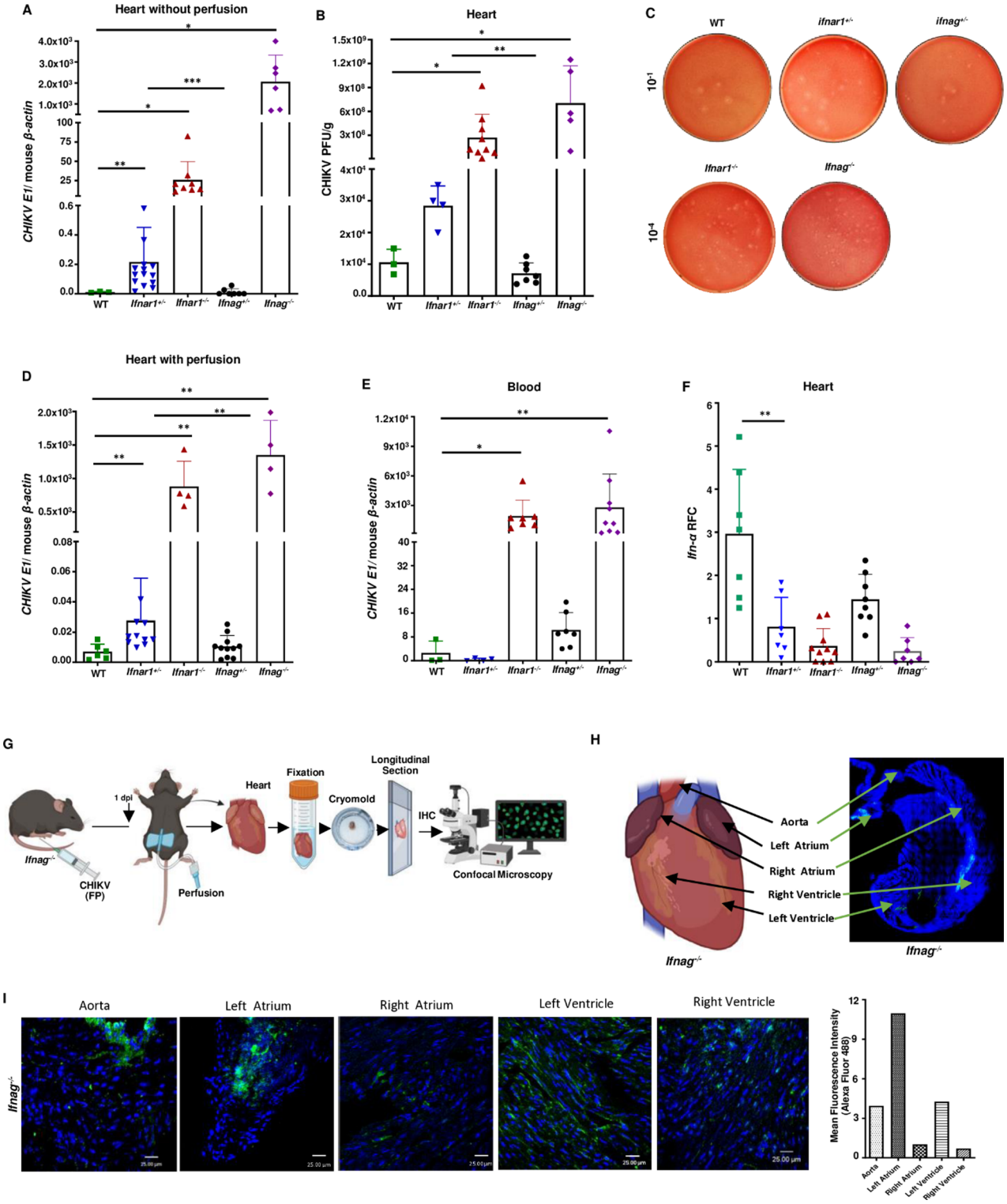

and 2 and becoming undetectable by D 9 p.i[32]. In our previous study, CHIKV load peaked at D1 p.i. in blood and footpads of WT, *il17a*$^{-/-}$, and *il17ra*$^{-/-}$ mice following footpad inoculation of CHIKV[8]. In addition, clinical studies reported that the early evidence of myocarditis could be observed as early as 5 days post-symptom onset in severe cases of CHIKV infection[12,33], while inflammation in hand tendons and the spleen has also been reported at a median as early as 4 days following illness onset in fatal cases of CHIKV infection[23]. In summary, our findings suggest that heterozygous mice (*ifnar1*$^{+/-}$ and *ifnag*$^{+/-}$) may be more suitable than homozygous *ifnar1*$^{-/-}$ and *ifnag*$^{-/-}$ mice for studying the mechanisms of CHIKV-caused heart diseases.

◀**Fig. 2**. IFN signaling is essential to control CHIKV infection in the heart. (**A**, **D**) The levels of *CHIKV E1* RNA presenting in the hearts of WT, *ifnar1*$^{-/-}$, *ifnar1*$^{+/-}$, *ifnag*$^{-/-}$, and *ifnag*$^{+/-}$mice on D1 p.i. were assessed using RT-qPCR in both non-perfused and perfused conditions. (**B**) The infectious CHIKV loads in the perfused heart tissues were measured by a plaque-forming assay on D1 p.i., and (**C**) The images of the representative viral plaques. (**E**) *CHIKV E1* RNA in the blood on D1 p.i. was quantified by RT-qPCR. (**F**) Expression of *Ifn-α* in CHIKV-infected hearts was analyzed using RT-qPCR. (**G**) Schematic representation of the immunohistochemistry (IHC) study in infected *ifnag*$^{-/-}$ mice. (**H**) The viral load was evaluated in different sections of the hearts of *ifnag*$^{-/-}$ mice after sectioning longitudinally. (**I**) The IHC staining with primary antibody, mouse monoclonal anti-Chikungunya virus antibody, secondary antibody, Alexa Fluor 488-conjugated goat anti-rat IgG (Green) (left), and the mean fluorescence intensity (right). The scale bars in the confocal images are 25 µm. Statistical analysis was conducted using one-way ANOVA followed by Tukey's test. Statistical significance is indicated as $*p < 0.05$, $**p < 0.01$, and $***p < 0.001$, respectively. (**G**, **H**) were created in BioRender. BAI, F. (2025) https://BioRender.com/o06u058, and https://BioRender.com/c33l008.

CHIKV infection increases the expression of cytokines and chemokines and neutrophil infiltration in the heart of heterozygous IFN signaling-deficient mice

Upon a virus infection, pattern recognition receptors (PRRs) of host cells recognize viral components, triggering the expression of pro-inflammatory cytokines and chemokines and recruiting immune cell infiltration to the infection site[34–36]. However, excessive cytokine production may also affect uninfected myocytes by promoting apoptosis, reducing contractility, and inducing cardiomyocyte hypertrophy[37,38]. We assessed the expression of the cytokines and chemokines, i.e., interleukin-6 (*Il-6*), interleukine-1β (*Il-1β*), tumor necrosis factor (*Tnf-α*), C-X-C motif chemokine ligand (*Cxcl*)1, *Cxcl2*, *Cxcl10*, and *Cxcl12* in CHIKV-infected *ifnar1*$^{+/-}$, *ifnag*$^{+/-}$, and WT mice on D1 p.i. (Fig. 4A). The RT-qPCR results revealed statistically higher expression of *Il-6*, *Il-1β*, *Cxcl2*, and *Cxcl12* in *ifnag*$^{+/-}$ mice than WT and 93-fold, 22-fold, 4-fold, 9-fold higher than *ifnar1*$^{+/-}$ respectively. Consistent with these results, the immunohistochemistry experiments showed a higher presence of CD45^{+} total leukocytes in the heart tissues of *ifnag*$^{+/-}$ than in *ifnar1*$^{+/-}$ and WT mice (Fig. 4B). Moreover, we quantified immune cell infiltration in the heart by flow cytometry and found that there were more neutrophils in the heart of *ifnag*$^{+/-}$ and *ifnar1*$^{+/-}$ mice than WT mice after CHIKV infection, with a trend that *ifnag*$^{+/-}$ mice exhibited more neutrophils over *ifnar1*$^{+/-}$ mice (Fig. 4C). Collectively, these results indicate that CHIKV infection increases the expression of cytokines and chemokines, and neutrophil infiltration in the heart of *ifnag*$^{+/-}$ and *ifnar1*$^{+/-}$ mice.

CHIKV infection leads to cardiac tissue damage and fibrosis in heterozygous IFN signaling-deficient mice

Human CHIKV infection in the heart can cause myocarditis, heart failure, and fibrosis. Fibrosis is the thickening and scarring of cardiac connective tissue due to excessive deposition of extracellular matrix proteins in the heart that can further impair heart function and lead to long-term complications both in humans and mice[39–41]. To evaluate the tissue damage due to CHIKV infection, we performed Hematoxylin and Eosin (H&E) staining on the heart tissues from CHIKV-infected *ifnag*$^{+/-}$, *ifnar1*$^{+/-}$, and WT mice. The H&E staining showed that *ifnag*$^{+/-}$ mice had more immune cell infiltration in the heart tissues than WT and *ifnar1*$^{+/-}$mice (Fig. 5A and B). The infiltration was primarily characterized by dense immune cell presence in the myocardium, especially in the left atrium, indicating active myocarditis and tissue damage (Fig. 5A). The severity of the infiltration and the associated tissue destruction was more pronounced in *ifnag*$^{+/-}$ mice compared to other groups (Fig. 5A). Further, vasculitis was observed in these mice from D1 p.i., characterized by thickened vessel walls due to immune cell infiltration. On D5 p.i., the vasculitis had further increased, highlighting a robust inflammatory response. The early onset of cell infiltration and inflammation observed in the *ifnag*$^{+/-}$ mice correlated with the higher expression of inflammatory cytokines and chemokines and the infiltration of neutrophils and other leukocytes (Fig. 4).

On the other hand, the *ifnar1*$^{+/-}$ mice displayed a delayed onset of tissue damage and myocarditis, which was visible on D5 p.i. (Fig. 5A). While vasculitis was evident early on D1 and D5 p.i., the overall severity was lower than the *ifnag*$^{+/-}$ mice. Another interesting observation was the vacuole formation with pyknosis (nuclear shrinkage) in the left ventricle in the *ifnar1*$^{+/-}$ mice (Fig. 5A). One study observed pyknosis (33%) in bone marrow tissues of CHIKV-infected IRF 3/7 double-deficient mice on D2 p.i[42]. In our study, the presence of vacuoles alongside pyknosis in the heart of *ifnar1*$^{+/-}$ mice might be due to a relatively higher and longer-lasting viral burden in *ifnar1*$^{+/-}$ mice than *ifnag*$^{+/-}$ and WT mice.

Fibrosis typically arises during the chronic phases of viral myocarditis, occurring as a result of prolonged inflammation and tissue damage[43]. Even after viral clearance, fibrotic remodeling may persist, reflecting an imbalance in tissue repair processes that leads to scarring and stiffening of the myocardium[41,44]. The early detection of fibrosis can be achieved by quantifying connective tissue growth factor (CTGF) expression using RT-qPCR, which provides higher sensitivity than conventional histological methods[45]. We measured *Ctgf* gene expression in the heart tissues of WT, *ifnag*$^{+/-}$, and *ifnar1*$^{+/-}$ mice on D1, D3, and D5 p.i. We found that *ifnar1*$^{+/-}$ mice displayed increased expression of *Ctgf* from D3 p.i. and exhibited significantly higher CTGF levels than WT and *ifnag*$^{+/-}$ mice (4-fold) on D5 p.i., indicating more severe fibrotic remodeling and cardiac damage in this group (Fig. 5C). These results also align with the viral burden results of the *ifnar1*$^{+/-}$ mice and the findings of a previous study, which demonstrated that the severity of the virus infection and impaired immune responses could intensify cardiac damage and promote fibrotic remodeling[46].

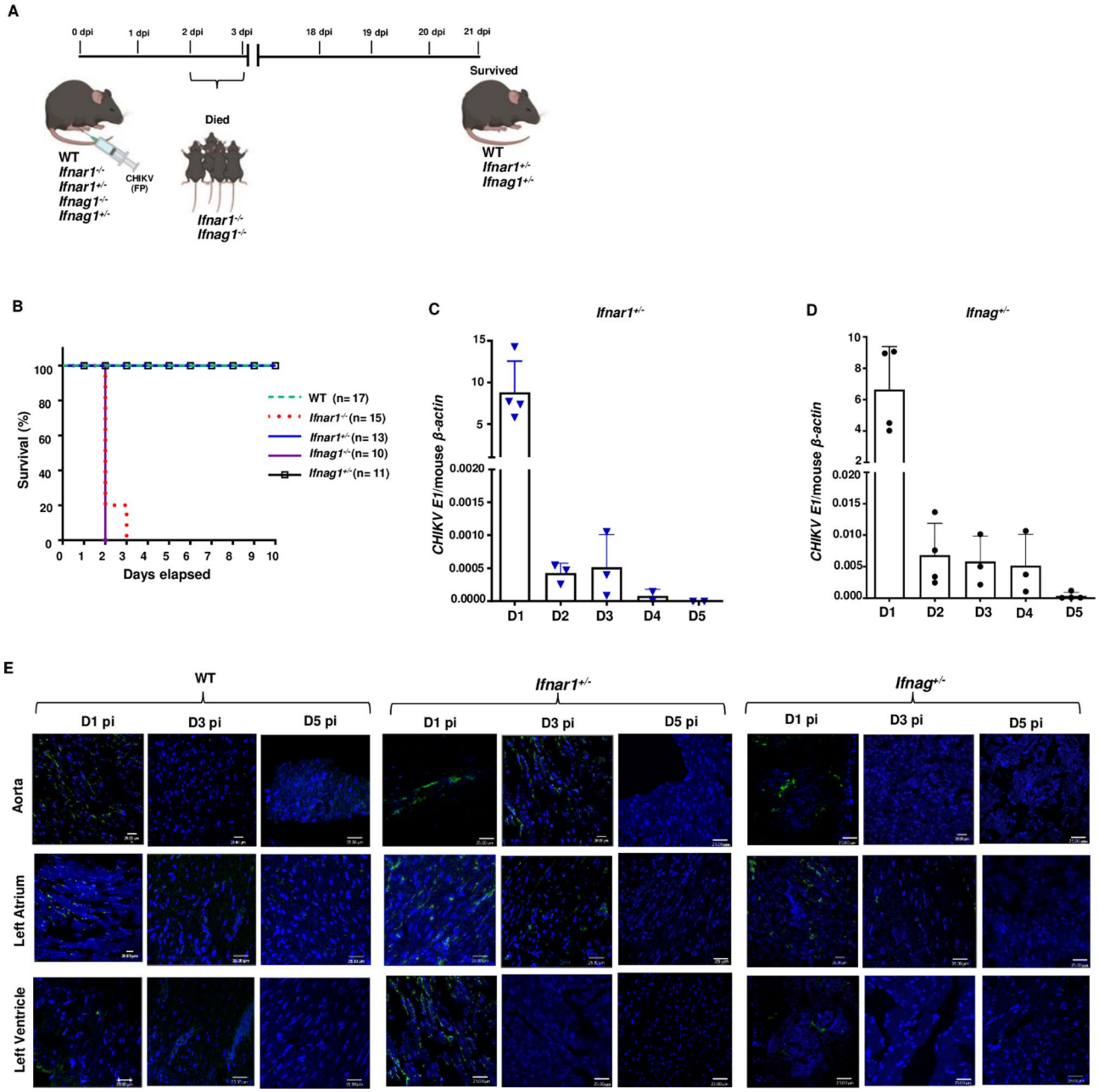

Fig. 3. Survival of the different types of IFN receptor knockout mice and the viral load in the hearts of *ifnag*$^{+/-}$ and *ifna*$^{+/-}$ mice after CHIKV infection. (**A**) Schematic representation of the survival study: WT, *ifnar1*$^{+/-}$, *ifnag*$^{+/-}$, *ifnar1*$^{-/-}$, and *ifnag*$^{-/-}$ mice were infected with CHIKV (1×10^5 PFU) via footpad and monitored daily for survival for 21 days (Created in BioRender. BAI, F. (2025) https://BioRender.com/c59p712). (**B**) The Kaplan-Meier survival curves. (**C** and **D**) RT-qPCR results of CHIKV E1 expression in the hearts of *ifnar1*$^{+/-}$and *ifnag*$^{+/-}$ mice. (**E**) The IHC staining with mouse monoclonal anti-Chikungunya virus antibody and Alexa Fluor 488-conjugated goat anti-rat IgG (Green) shows the presence/ absence of virus in the aorta, left atrium, and left ventricle on D1, 3, and 5 p.i. among WT, *ifnar1*$^{+/-}$, and *ifnag*$^{+/-}$ mice.

In summary, these results suggest that CHIKV infection leads to cardiac tissue damage and fibrosis in heterozygous IFN signaling-deficient mice, especially in *ifnar1*$^{+/-}$ mice, possibly due to the relatively higher and prolonged viral burden in the heart tissues.

Discussion

Innate immune response, including IFN production, is the frontline of host defense against viral infections[47–49]. The pathogen-associated molecular patterns (PAMPS) of RNA viruses are recognized by pattern-recognition receptors (PRRs) of the host cells, triggering a signaling cascade and activating transcription factors, which leads to the production of type I IFNs, including IFN-α and IFN-β, and pro-inflammatory cytokines[50]. Type I IFNs are

crucial in inhibiting viral replication[51] and type II interferon, specifically IFN-γ, has diverse immune regulatory roles, including antiviral activities, activation of immune cells, and regulation of immune responses[52]. IFN-α/β initiate their antiviral activities by binding to their specific cell surface receptors (IFNAR1/IFNAR2), and type II IFNs (IFN-γ) function by binding to IFNGR1/IFNGR2 receptors[53]. When IFNs bind to their cellular receptors, the Janus Kinases (JAK1 and TYK2) - Signal Transducers and Activators of Transcription (STAT1 and STAT2) signaling pathways are activated. This leads to the formation of the interferon-stimulated gene factor 3 (ISGF3) complex in type I IFN signaling and the gamma interferon activation factor (GAF) in type II IFN signaling[54,55]. Both ISGF3 and GAF activate specific genes to induce the expression of interferon-stimulated genes (ISGs) that play vital roles in antiviral defense[54,56].

The activation of a type I interferon (IFN) response has been documented in cardiomyopathy and viral (SARS-CoV-2, Coxsackievirus) cardiovascular complications, where it predominantly exerts protective effects by modulating immune activity both in humans and mice[57,58]. Additionally, studies have identified type II interferon (IFN-γ) as a crucial regulator of immune cell recruitment and inflammation in myocardial infarction in murine models[59]. However, the impact of type I and type II IFN response is not always beneficial, as they may sometimes play a detrimental role in facilitating heart injury in certain pathological contexts[60,61]. A recent study found auto-antibodies against type I IFNs in severe COVID-19 patients, suggesting a potential role for IFN dysregulation is also involved in virus-induced complications, including CVD[62]. CHIKV infection has been shown to induce robust type I interferon production, which is indispensable for the host's initial defense against viral replication[63,64]. In our study, we found that suckling WT mice were relatively susceptible to CHIKV infection in the heart and then became resistant when they grew older. Similarly, severe CHIKV infection was observed in muscles, joints, and skin in neonatal WT mice and human infants[27,29]. This may be due to the maturing status of the immune system, especially the IFN pathways, during development. The homozygous interferon receptor-deficient (*ifnar1*$^{-/-}$ and *ifnag*$^{-/-}$) mice exhibited significantly higher viral burden in the heart compared to WT mice at the same age; however, all these animals died between 2 and 3 days after infection, indicating these animals may not be suitable for studying CHIKV-caused heart diseases. Nevertheless, this finding confirms that IFN signaling is critical in controlling CHIKV replication in the heart and other organs and protecting the mice from death. The in vitro studies have also demonstrated that CHIKV replication is significantly reduced by adding type I and type II interferons[65,66]. Furthermore, an in vivo study has found that IFN-knockout mice exhibited more severe disease outcomes compared to WT mice after the same amount of CHIKV infection[67]. In particular, the absence of type I (IFN-α/β) and type II (IFN-γ) responses in homozygous mice severely compromised their ability to mount an effective antiviral response, leading to unchecked viral replication and dissemination[68]. Interestingly, we discovered that CHIKV did not uniformly infect the parts of the heart, with higher viral burden in the left atrium, left ventricle, and aorta compared to the right ventricle and right atrium. This is consistent with a previous study that observed significant infection in the upper part of the heart, including the atrium and aorta, more vascularized regions of the heart[32]. The increased vascularization in these areas likely contributes to higher viral exposure, making them more vulnerable to CHIKV infection.

Compared to the homozygous interferon receptor-deficient (*ifnar1*$^{-/-}$ and *ifnag*$^{-/-}$) mice, the heterozygous mice (*ifnar1*$^{+/-}$ and *ifnag*$^{+/-}$) showed a reduced viral load in the heart, with a 100% survival rate without showing any apparent disease symptoms until the end of the experiments. The reduced viral burden and improved survival in the heterozygous mice imply that a threshold level of IFN signaling is required for coordinating an effective immune response. The inflammatory response during a viral infection is closely linked to the infection status and immune cell filtration. The cytokine expression profiles during infection of cardiotropic viruses are not well characterized and vary depending on the virus involved[37]. Our findings in this study suggest the significant roles of the pro-inflammatory cytokines in the immune response to CHIKV infection in the heart of *ifnar1*$^{+/-}$, *ifnag*$^{+/-}$, and WT mice. Higher levels of cytokines, such as *Il-6*, *Il-1β*, and chemokines *Cxcl1*, *Cxcl2*, and *Cxcl12*, were detected in the heart of the infected *ifnag*$^{+/-}$ mice than *ifnar1*$^{+/-}$ and WT mice. These cytokines and chemokines play critical roles in recruiting immune cells, such as neutrophils and monocytes, to the site of infection for viral clearance[37,69,70]. Flow cytometry and IHC analysis confirmed an increase in neutrophil and total leukocyte infiltration in the heart tissue of *ifnag*$^{+/-}$ mice. In a murine model of viral myocarditis, an early and abundant infiltration of neutrophils into the heart between 2 and 3 days following Coxsackievirus B3 (CVB3) infection has also been reported[69,71]. The early neutrophil recruitment likely contributed to the rapid viral clearance from the heart of *ifnag*$^{+/-}$ mice. However, the infiltrated leukocytes can also lead to cardiac damage to both infected and uninfected heart tissues[37,72]. Our histological analysis revealed significant immune cell infiltration and myocarditis, particularly in the left atrium and left ventricle of *ifnag*$^{+/-}$ mice, with evidence of necrosis and vasculitis. These findings suggest that while the immune response in *ifnag*$^{+/-}$ mice is protective for viral replication, excessive inflammation can cause collateral damage to the heart if not properly regulated. The balance between viral clearance and minimizing tissue damage is crucial in preventing long-term cardiac dysfunction during CHIKV infection. Future studies are warranted to investigate the long-term cardiac outcomes post-CHIKV infection in these mice.

The delayed onset of tissue damage and myocarditis in *ifnar1*$^{+/-}$ mice, as observed on D5 p.i., implies a distinct immune response profile compared to *ifnag*$^{+/-}$ mice. The early signs of vasculitis noted on D1 and persisting through D5 p.i., were less severe in the *ifnar1*$^{+/-}$ mice, suggesting a constrained inflammatory response in the early stage of the infection. However, vacuole formation and pyknosis in the left ventricle of *ifnar1*$^{+/-}$ mice suggest that these mice experienced more pronounced tissue damage than the *ifnag*$^{+/-}$group. This finding aligns with a previous study, which reported CHIKV-induced pyknosis in the tissues of IRF3/7 double deficient mice on D2 p.i[42]. More importantly, the elevated CTGF levels on D5 p.i. in *ifnar1*$^{+/-}$ mice indicate a sign of myocardial fibrosis compared to WT and *ifnag*$^{+/-}$ mice, confirming that CHIKV infection induces chronic tissue damage in the heart that may lead to arrhythmias, myocardial infarction, and heart failure in *ifnar1*$^{+/-}$ mice[74]. These findings suggest that a less efficient early-stage immune response may allow for prolonged viral persistence and

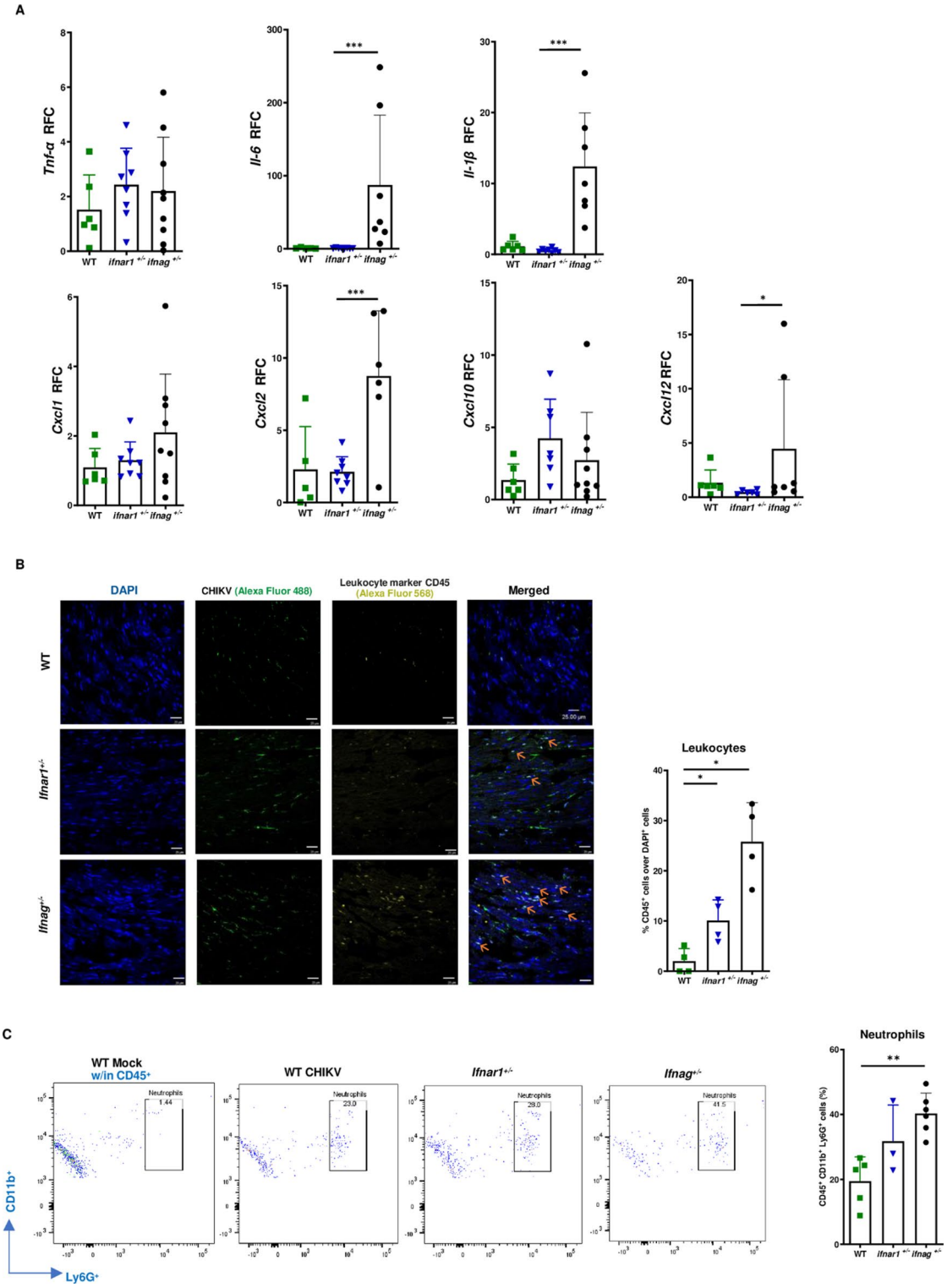

subsequent heart tissue damage, emphasizing the critical importance of early treatment of viral replication in mitigating CHIKV-caused heart diseases in humans.

In conclusion, our results demonstrate that the signaling of type I and II interferons is essential in controlling CHIKV infection in the heart. Despite the slight differences in responding to CHIKV infection, *ifnag*$^{+/-}$and *ifnar1*$^{+/-}$mice may be suitable animal models to study the mechanisms and test therapeutic interventions for CHIKV-caused cardiac diseases.

Methods

Ethics statement and biosafety

All the experiments involving live chikungunya virus (CHIKV) were carried out by trained and certified personnel in the USDA-certified Biosafety Level 3 (BSL3) facilities at the University of Southern Mississippi

◀**Fig. 4**. Increase the expression of cytokines, chemokines, and neutrophil infiltration in the hearts of CHIKV-infected *ifnag*$^{+/-}$ mice. WT, *ifnar1*$^{+/-}$, and *ifnag*$^{+/-}$ mice were infected with CHIKV (1×10^5 PFU) via footpad, and the hearts were collected on D1 p.i. after perfusion. (**A**) The RT-qPCR analysis of the expression of *Tnf-α*, *Il-6*, *Il-1β*, *Cxcl1*, *Cxcl2*, *Cxcl10*, and *Cxcl12* in the hearts. (**B**-left) Immunohistochemistry of the heart sections of WT, *ifnar1*$^{+/-}$, and *ifnag*$^{+/-}$ mice stained with DAPI (blue, for nuclei), Alexa Fluor 488 (green, for anti-Chikungunya virus antibody), Alexa Fluor 568 (yellow, for leukocyte marker CD45), and observed under a confocal microscope at 20× magnification. Colocalizations of CHIKV E1 and CD45 are marked by orange arrows. The scale bars of all images are 25 µm. (**B**-right) Quantification of CD45$^+$ cells in a bright field of confocal images. (**C**-left) Flow cytometry results of the neutrophil infiltration in the hearts of WT, *ifnar1*$^{+/-}$, and *ifnag*$^{+/-}$ mice. The infiltrated neutrophils are defined as CD45$^+$ CD11b$^+$Ly6G$^+$ cells. (**C**-right) Quantification of the infiltrated neutrophils in the hearts. The data presented are from at least two independent experiments performed in triplicate. Statistical analysis was conducted using one-way ANOVA followed by Tukey's test. Statistical significance is indicated as $^*p < 0.05$ and $^{***}p < 0.001$.

(USM) by following the biosafety protocol approved by the USM Institutional Biosafety Committee. The animal experiments in this study were reviewed and approved by the Institutional Animal Care and Use Committees (IACUC) at USM under the IACUC protocols # 15,101,601 and 17,110,903. The mice were anesthetized under 25% v/v isoflurane and euthanized in a high CO_2 environment. These procedures comply with the recommended practices of the Panel on Euthanasia of the American Veterinary Medical Association (AVMA). All authors comply with the ARRIVE guidelines, and all methods followed the relevant guidelines and regulations.

Viruses and cells

The CHIKV (LR OPY1 2006 strain) was supplied by the World Reference Center for Emerging Viruses and Arboviruses at the University of Texas Medical Branch. A single passage of the parental viruses was cultivated in Vero cells (ATCC CCL-81) and employed as the viral stock. The titration of viral stocks was determined in Vero cells using a plaque-forming assay[8,74]. Vero cells were maintained in Dulbecco's Modified Eagle Medium (Gibco™ DMEM, Life Technologies) containing 1% L-glutamine, 1% Penicillin/Streptomycin, and 10% fetal bovine serum.

Mice and animal study

Breeding pairs of wild-type (WT, C57BL/6J, Strain #: 000664), *ifnar1*$^{-/-}$ (Strain #:028288), and *ifnag* $^{-/-}$ (Strain #:029098) mice on a C57BL/6J background were obtained from The Jackson Laboratory (Bar Harbor, ME). Heterozygous *ifnar1*$^{+/-}$ and *ifnag*$^{+/-}$ mice were generated by crossing respective homozygous mice with WT mice. All breeding pairs and their offspring were housed in a clean facility, and the CHIKV infection experiments were conducted in the BSL-3 laboratory. For CHIKV infection, mice were subcutaneously injected with 1×10^5 PFU in phosphate-buffered saline (PBS) into the ventral side of the left hind footpad. In the survival experiments, mice were observed daily for morbidity and mortality for 21 days. Blood samples were collected from the retro-orbital sinus on D1 p.i. to measure viremia by RT-qPCR. The hearts and spleens were collected on various days p.i., for analysis by RT-qPCR, plaque-forming assays, flow cytometry, and immunohistochemistry. The body weight and the weight of the heart were monitored on different days p.i.

Reverse-transcription quantitative real-time PCR (RT-qPCR)

The blood, spleen, and heart samples were collected, and total RNA was extracted with TRI-Reagent. The first-strand complementary DNA (cDNA) was synthesized using an iSCRIPT cDNA synthesis kit (Bio-Rad). RT-qPCR was performed in a CFX Connect Real-Time System (Bio-Rad) using iTaq universal probes Supermix (Bio-Rad) to detect *CHIKV-E1* and mouse cellular *β-actin*. Viral RNA copy numbers were expressed as the ratio of *CHIKV-E1* to *β-actin*. Relative fold change (RFC) to the control was done using the comparative threshold cycle $^{\Delta\Delta}$CT method after normalizing to cellular *β-actin*. *CHIKV-E1* and cellular *β-actin* gene primers and probe sequences were adapted according to previous publications: *CHIKV-E1*[8] and *β-actin*[75–78]. The list of all primers used in this study is provided in Table 1.

Plaque-forming assay

Vero cells were seeded in 6-well plates at a density of 6×10^5 cells per well and incubated overnight. Supernatants collected after centrifugation of homogenized heart and blood samples were serially diluted and then applied to the monolayers of Vero cells. After 1 h of incubation at 37 °C with 5% CO_2, the virus inoculum was removed, and the cell monolayer was covered with an overlay medium containing 1% SeaPlaque agarose (Lonza). The plates were incubated for 24 to 48 h at 37 °C with 5% CO_2 until plaques were formed. The plaques were counted after staining with Neutral Red for 3 h. The viral titers were calculated in plaque-forming units per milliliter (PFU/ml) following the formula described in previous studies[78–80].

Flow cytometry

Three-week-old WT, *ifnar1*$^{+/-}$ and *ifnag*$^{+/-}$ mice were inoculated with 1×10^5 PFU of CHIKV or PBS (control) via footpad injection. The mice were perfused, and the hearts were collected on day 1 p.i. The hearts were minced into small pieces and digested with a collagenase cocktail (DNase I (Thermo Scientific), HEPES (Gibco™), and collagenase (Sigma)) on a rotating shaker for 45 min at 37°C. The cardiac cells were centrifuged at 393 g for 5 minutes at 4°C, the supernatant was discarded, and the pellet was resuspended in 3 ml of Hank's Balanced Salt Solution (HBSS, Gibco™). The suspension was filtered through a 40 µm cell strainer for surface staining.

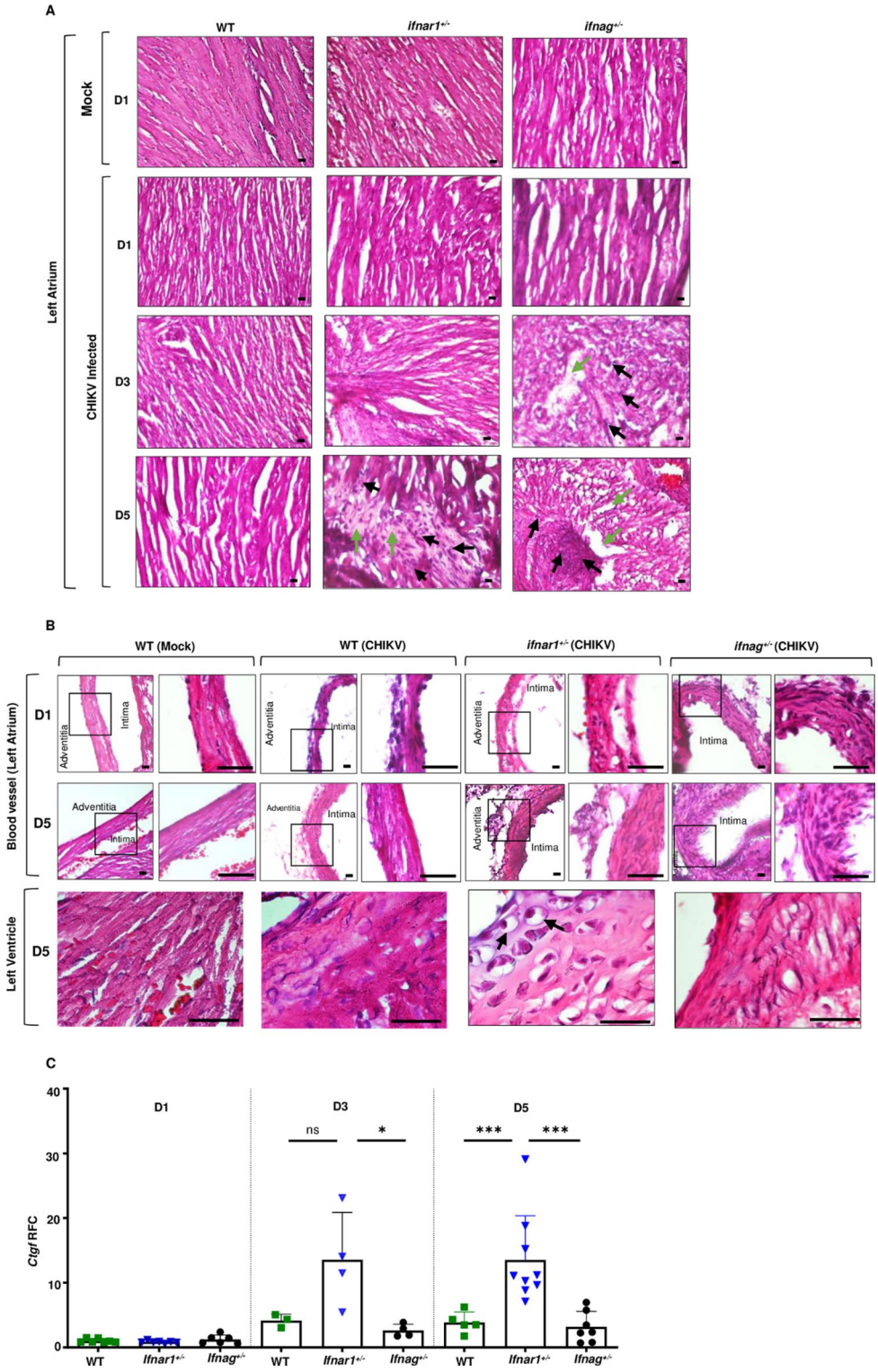

Fig. 5. Histological analysis of myocardial tissues of CHIKV-infected WT, *ifnar1*$^{+/-}$, and *ifnag*$^{+/-}$ mice. WT, *ifnar1*$^{+/-}$, and *ifnag*$^{+/-}$ mice were infected with CHIKV (1×10^5 PFU) via footpad, and the hearts were collected on D1 p.i. (**A**) The representative H&E-stained sections of the left atria from WT, *ifnar1*$^{+/-}$, and *ifnag*$^{+/-}$ mice showing immune cell infiltrations (black arrow) and tissue damage (green arrow). (**B**) H&E-stained sections of the left atria highlighting the vasculitis in the left ventricles on D5 p.i. in both heterozygous groups and the vacuole formation and pyknosis in *ifnar1*$^{+/-}$ mice (arrow) compared to other groups. The scale bars of all images are 100 µm. (**C**) The connective tissue growth factor (CTGF) expression is evaluated by QPCR as RFC for potential fibrosis development in WT, *ifnar1*$^{+/-}$, and *ifnag*$^{+/-}$ mice. Statistical significance is indicated as $^{***}p < 0.001$.

Primer	Forward 5′–3′	Reverse 5′–3′
mβ-actin	AGA GGG AAA TCG TGC GTG AC	CAA TAG TGA TGA TGA CCT GGC CGT
CHIKV E1	TCC GGG AAG CTG AGA TAG AA	ACG CCG GGT AGT TGA CTA TG
m*Tnf-α*	CAG GCG GTG CCT ATG TCT C	CGA TCA CCC CGA AGT TCA GTA G
m*Il-6*	TAG TCC TTC CTA CCC CAA TTT CC	TTG GTC CTT AGC CAC TCC TTC
m*Il-1β*	TGG TGT GTG ACG TTC CCA TT	CAG CAC GAG GCT TTT TTG TTG
m*Cxcl1*	TGC ACC CAA ACC GAA GTC AT	ACT TGG GGA CAC CTT TTA GCA
m*Cxcl2*	GCG CCC AGA CAG AAG TCA TA	CAG TTA GCC TTG CCT TTG TTC A
m*Cxcl10*	GCC GTC ATT TTC TGC CTC A	CGT CCT TGC GAG AGG GAT
m*Cxcl12*	CAG AGC CAA CGT CAA GCA	AGG TAC TCT TGG ATC CAC
m*Ctgf*	GGG CCT CTT CTG CGA TTT C	ATC CAG GCA AGT GCA TTG GTA
m*Ifn-α*	AGG ACA GGA AGG ATT TTG GA	GCT GCT GAT GGA GGT CAT T

Table 1. Primer sequences used for RT-qPCR.

The heart-infiltrated leukocytes were probed with antibodies CD45 (PE-Cy7-conjugated, eBioscience), CD11b (APC-conjugated, BD Biosciences), and Ly6G (APC Cy7-conjugated, Invitrogen). The samples were processed using the BD LSRFortessa™ Cell analyzer (BD Biosciences), and the data were analyzed with FlowJo (v10.9.0.) software.

Immunohistochemistry

Three-week-old mice of WT, *ifnar1*$^{-/-}$, *ifnag*$^{-/-}$, *ifnar1*$^{+/-}$, and *ifnag*$^{+/-}$ were infected with 1×10^5 PFU of CHIKV via footpad injection. On day 1 p.i., the hearts were collected after perfusion and fixed in 4% paraformaldehyde (PFA) and cryoprotected sequentially in 20% and 30% sucrose for 24 h at 4 °C. Following cryoprotection, the hearts were placed on a Tissue-Tek tray (Sakura Finetek USA, Inc.), embedded in optimal cutting temperature (OCT) compound (Fisher HealthCare), and snap-frozen in liquid nitrogen before being stored overnight at a -80 °C freezer. Longitudinal heart sections were cut at a thickness of 10 µm using a cryostat (Tissue-Tek® Cryo3, Sakura), mounted on charged glass slides (Fisher Scientific), and air-dried overnight. The sections were then treated with 200 µl of antigen retrieval solution, followed by blocking with 2% goat serum containing 0.3% Triton X-100 and 0.05% Tween-20 in PBS for 1 h at room temperature. Then, the sections were probed overnight at 4°C with the following primary antibodies: mouse monoclonal anti-Chikungunya virus antibody (1:100, Cat # ab155841, Abcam); rabbit monoclonal Ly-6G antibody (1:100, Cat # 6O10Y1, Invitrogen); rabbit CD45 recombinant antibody (1:100, Cat # 80297-1-RR, Proteintech). After washing 3–5 times with PBS, the sections were stained with secondary antibodies: Alexa Fluor 488-conjugated goat anti-rat IgG (H + L) (1:100, Cat # 112-545-003, Jackson ImmunoResearch) for anti-CHIKV primary antibody; Alexa Fluor 568-conjugated goat anti-rabbit IgG (1:100, Invitrogen, A-11011) for either Ly6G or CD45 primary antibodies for 2 h at 4°C. The sections were washed 3–5 times with PBS and covered with mounting media with DAPI (4′, 6-diamidino-2-phenylindole, Vector Laboratories, Inc. Burlingame, CA). The images were captured using a Stellaris STED confocal microscope (Leica). This protocol was adapted from previously published methods[79,81,82].

Hematoxylin and Eosin staining

Pathological examination of heart tissue was performed using a Hematoxylin and Eosin (H&E) Staining Kit (Cat # ab245880, Abcam). Heart samples were embedded in OCT compound and sectioned longitudinally at a thickness of 10 µm. Sections were hydrated in distilled water and subsequently immersed in Hematoxylin (Modified Mayer's Solution) for 5 min. Then, the slides were rinsed twice in distilled water and immersed in a bluing reagent for 15 s. The slides were washed in two changes of distilled water and briefly dipped in 95% ethanol. Then, the tissue sections were stained with Eosin Y Solution for 2 min. The sections were then dehydrated in one change of 95% ethanol and three changes of 100% ethanol briefly. Finally, the slides were mounted (Surgipath Micromount, Leica) with a coverslip. This staining protocol was adapted from previously published methods[8,83]. The images were captured by the Nikon Eclipse 80i microscope (Nikon, Japan) at different magnifications (10×, 20×, 40×, and 100×).

Statistical analysis

If not mentioned, all data were generated using triplicates. Data were analyzed using the Mann Whitney U test, log-rank test, or one/two-tailed student's t-tests with the GraphPad Prism software (version 10.2.3), whichever was applicable.

Data availability

All data generated or analyzed during this study are included in this published article.

Received: 26 November 2024; Accepted: 12 May 2025
Published online: 23 May 2025

References

1. Alvarez, M. F., Bolivar-Mejia, A., Rodriguez-Morales, A. J. & Ramirez-Vallejo, E. Cardiovascular involvement and manifestations of systemic Chikungunya virus infection: A systematic review. *F1000Res* **6**, 390 (2017).
2. Traverse, E. M., Hopkins, H. K., Vaidhyanathan, V. & Barr, K. L. Cardiomyopathy and death following Chikungunya infection: an increasingly common outcome. *Trop Med. Infect. Dis* **6** (2021).
3. Suhrbier, A., Jaffar-Bandjee, M. C. & Gasque, P. Arthritogenic alphaviruses–an overview. *Nat. Rev. Rheumatol.* **8**, 420–429 (2012).
4. Staples, J. E. & Fischer, M. Chikungunya virus in the Americas–what a vectorborne pathogen can do. *N Engl. J. Med.* **371**, 887–889 (2014).
5. Mohapatra, R. K. et al. Global health concern on the rising dengue and Chikungunya cases in the American regions: countermeasures and preparedness. *Health Sci. Rep.* **7**, e1831 (2024).
6. Kayange, N. et al. Seroprevalence of dengue and Chikungunya virus infections in children living in Sub-Saharan Africa: systematic review and meta-analysis. *Children* **10**, 1662 (2023).
7. Gibney, K. B. et al. Chikungunya fever in the united States: a fifteen year review of cases. *Clin. Infect. Dis.* **52**, e121–126 (2011).
8. Neupane, B. et al. Interleukin-17A facilitates Chikungunya virus infection by inhibiting IFN-alpha2 expression. *Front. Immunol.* **11**, 588382 (2020).
9. Burt, F. J. et al. Chikungunya virus: an update on the biology and pathogenesis of this emerging pathogen. *Lancet Infect. Dis.* **17**, e107–e117 (2017).
10. Cotella, J. I. et al. *Chikungunya Heart Cardiology* **146**, 324–334 (2021).
11. Schwartz, O. & Albert, M. L. Biology and pathogenesis of Chikungunya virus. *Nat. Rev. Microbiol.* **8**, 491–500 (2010).
12. Acosta-Reyes, J. et al. High levels of cardiovascular biomarkers in fatal Chikungunya virus infection. *Acta Trop.* **237**, 106705 (2023).
13. Tandale, B. V. et al. Systemic involvements and fatalities during Chikungunya epidemic in India, 2006. *J. Clin. Virol.* **46**, 145–149 (2009).
14. Sa, P. K. O. et al. Chikungunya virus infection with severe neurologic manifestations: report of four fatal cases. *Rev. Soc. Bras. Med. Trop.* **50**, 265–268 (2017).
15. Torres, J. R. et al. Congenital and perinatal complications of Chikungunya fever: a Latin American experience. *Int. J. Infect. Dis.* **51**, 85–88 (2016).
16. Villamil-Gomez, W. et al. Congenital Chikungunya virus infection in Sincelejo, Colombia: A case series. *J. Trop. Pediatr.* **61**, 386–392 (2015).
17. Mason, J. W. Myocarditis and dilated cardiomyopathy: an inflammatory link. *Cardiovasc. Res.* **60**, 5–10 (2003).
18. Schultz, J. C., Hilliard, A. A., Cooper, L. T. Jr. & Rihal, C. S. Diagnosis and treatment of viral myocarditis. *Mayo Clin. Proc.* **84**, 1001–1009 (2009).
19. London, B. Immune modulation of cardiac arrhythmias. *Circ. Res.* **121**, 11–12 (2017).
20. Traverse, E. M. et al. Chikungunya immunopathology as it presents in different organ systems. *Viruses* **14** (2022).
21. Mallilankaraman, K. et al. A DNA vaccine against Chikungunya virus is protective in mice and induces neutralizing antibodies in mice and nonhuman primates. *PLoS Negl. Trop. Dis.* **5**, e928 (2011).
22. Ngwe Tun, M. M. et al. Pathogenetic Potential Relating to Metabolic Activity in a Mouse Model of Infection with the Chikungunya Virus East/Central/South African Genotype. *Viruses* 12 (2020).
23. Sharp, T. M. et al. Clinical characteristics, histopathology, and tissue immunolocalization of Chikungunya virus antigen in fatal cases. *Clin. Infect. Dis.* **73**, e345–e354 (2021).
24. Zhang, H. L. et al. Visualization of Chikungunya virus infection in vitro and in vivo. *Emerg. Microbes Infect.* **8**, 1574–1583 (2019).
25. Simon, F. et al. Chikungunya: risks for travellers. *J Travel Med* **30** (2023).
26. Iwamura, T., Guzman-Holst, A. & Murray, K. A. Accelerating invasion potential of disease vector Aedes aegypti under climate change. *Nat. Commun.* **11**, 2130 (2020).
27. Couderc, T. et al. A mouse model for Chikungunya: young age and inefficient type-I interferon signaling are risk factors for severe disease. *PLoS Pathog*. **4**, e29 (2008).
28. De, S. et al. MBZM-N-IBT, a novel small molecule, restricts Chikungunya virus infection by targeting nsP2 protease activity in vitro, in vivo, and ex vivo. *Antimicrob. Agents Chemother.* **66**, e0046322 (2022).
29. Gerardin, P. et al. Multidisciplinary prospective study of mother-to-child Chikungunya virus infections on the Island of La reunion. *PLoS Med.* **5**, e60 (2008).
30. Venugopalan, A., Ghorpade, R. P. & Chopra, A. Cytokines in acute Chikungunya. *PLoS One.* **9**, e111305 (2014).
31. Chaaitanya, I. K. et al. Role of Proinflammatory cytokines and chemokines in chronic arthropathy in CHIKV infection. *Viral Immunol.* **24**, 265–271 (2011).
32. Noval, M. G. et al. MAVS signaling is required for preventing persistent Chikungunya heart infection and chronic vascular tissue inflammation. *Nat. Commun.* **14**, 4668 (2023).
33. Menon, P. R., Sankar, J., Gopinathan, K. & Mohan, G. A child with serious Chikungunya virus (CHIKV) infection requiring intensive care, after an outbreak. *Indian J. Pediatr.* **77**, 1326–1328 (2010).
34. Karim, S. U. & Bai, F. Introduction to West nile virus. *Methods Mol. Biol.* **2585**, 1–7 (2023).
35. Kawai, T. & Akira, S. The role of pattern-recognition receptors in innate immunity: update on Toll-like receptors. *Nat. Immunol.* **11**, 373–384 (2010).
36. Wang, L. L. et al. Identification of Benzothiophene-Derived inhibitors of flaviviruses by targeting RNA-Dependent RNA polymerase. *Viruses* **17**, 145 (2025).
37. Martens, C. R. & Accornero, F. Viruses in the heart: direct and indirect routes to myocarditis and heart failure. *Viruses* 13 (2021).
38. Akhmerov, A. & Marbán, E. COVID-19 and the heart. *Circul. Res.* **126**, 1443–1455 (2020).
39. Bacmeister, L. et al. Inflammation and fibrosis in murine models of heart failure. *Basic Res. Cardiol.* **114**, 1–35 (2019).
40. Kruszewska, J., Cudnoch-Jedrzejewska, A. & Czarzasta, K. Remodeling and fibrosis of the cardiac muscle in the course of Obesity-Pathogenesis and involvement of the extracellular matrix. *Int J. Mol. Sci* **23** (2022).
41. Talman, V. & Ruskoaho, H. Cardiac fibrosis in myocardial infarction-from repair and remodeling to regeneration. *Cell. Tissue Res.* **365**, 563–581 (2016).
42. Goupil, B. A. et al. Novel lesions of bones and joints associated with Chikungunya virus infection in two mouse models of disease: new insights into disease pathogenesis. *PLoS One.* **11**, e0155243 (2016).
43. Pollack, A., Kontorovich, A. R., Fuster, V. & Dec, G. W. Viral myocarditis–diagnosis, treatment options, and current controversies. *Nat. Rev. Cardiol.* **12**, 670–680 (2015).
44. Ammirati, E. et al. Clinical presentation and outcome in a contemporary cohort of patients with acute myocarditis: multicenter Lombardy registry. *Circulation* **138**, 1088–1099 (2018).
45. Syed, M. et al. MicroRNA-21 ablation exacerbates aldosterone-mediated cardiac injury, remodeling, and dysfunction. *Am. J. Physiol. Endocrinol. Metab.* **315**, E1154–E1167 (2018).
46. Boehme, K. W. & Compton, T. Innate sensing of viruses by toll-like receptors. *J. Virol.* **78**, 7867–7873 (2004).
47. Sen, G. C. Viruses and interferons. *Annu. Rev. Microbiol.* **55**, 255–281 (2001).
48. Suzuki, Y. Interferon-induced restriction of Chikungunya virus infection. *Antiviral Res.* **210**, 105487 (2023).
49. Dey, S. Molecular epidemiology of influenza in Asia. *Eastern J. Med.* **19**, 119–125 (2014).
50. Kell, A. M. & Gale, M. Jr RIG-I in RNA virus recognition. *Virology* **479**, 110–121 (2015).

51. Crouse, J., Kalinke, U. & Oxenius, A. Regulation of antiviral T cell responses by type I interferons. *Nat. Rev. Immunol.* **15**, 231–242 (2015).
52. Platanias, L. C. Mechanisms of type-I-and type-II-interferon-mediated signalling. *Nat. Rev. Immunol.* **5**, 375–386 (2005).
53. Negishi, H., Taniguchi, T. & Yanai, H. The interferon (IFN) class of cytokines and the IFN regulatory factor (IRF) transcription factor family. *Cold Spring Harb Perspect. Biol* **10** (2018).
54. Schneider, W. M., Chevillotte, M. D. & Rice, C. M. Interferon-stimulated genes: a complex web of host defenses. *Annu. Rev. Immunol.* **32**, 513–545 (2014).
55. Stark, G. R. & Darnell, J. E. Jr. The JAK-STAT pathway at Twenty. *Immunity* **36**, 503–514 (2012).
56. Wesoly, J., Szweykowska-Kulinska, Z. & Bluyssen, H. A. STAT activation and differential complex formation dictate selectivity of interferon responses. *Acta Biochim. Pol.* **54**, 27–38 (2007).
57. Althof, N. et al. In vivo ablation of type I interferon receptor from cardiomyocytes delays coxsackieviral clearance and accelerates myocardial disease. *J. Virol.* **88**, 5087–5099 (2014).
58. Miric, M., Miskovic, A., Vasiljevic, J. D., Keserovic, N. & Pesic, M. Interferon and thymic hormones in the therapy of human myocarditis and idiopathic dilated cardiomyopathy. *Eur. Heart J.* **16** (Suppl O), 150–152 (1995).
59. Finger, S. et al. A sequential interferon gamma directed chemotactic cellular immune response determines survival and cardiac function post-myocardial infarction. *Cardiovasc. Res.* **115**, 1907–1917 (2019).
60. King, K. R. et al. IRF3 and type I interferons fuel a fatal response to myocardial infarction. *Nat. Med.* **23**, 1481–1487 (2017).
61. Duley, A. K. et al. Negative impact of IFN-gamma on early host immune responses to retroviral infection. *J. Immunol.* **189**, 2521–2529 (2012).
62. Bastard, P. et al. Autoantibodies against type I IFNs in patients with life-threatening COVID-19. *Science* **370** (2020).
63. Gifford, G. E. & Heller, E. Effect of actinomycin D on interferon production by 'active' and 'inactive' Chikungunya virus in chick cells. *Nature* **200**, 50–51 (1963).
64. Her, Z. et al. Active infection of human blood monocytes by Chikungunya virus triggers an innate immune response. *J. Immunol.* **184**, 5903–5913 (2010).
65. Briolant, S., Garin, D., Scaramozzino, N., Jouan, A. & Crance, J. M. In vitro Inhibition of Chikungunya and Semliki forest viruses replication by antiviral compounds: synergistic effect of interferon-alpha and ribavirin combination. *Antiviral Res.* **61**, 111–117 (2004).
66. Sourisseau, M. et al. Characterization of reemerging Chikungunya virus. *PLoS Pathog.* **3**, e89 (2007).
67. Cook, L. E. et al. Distinct roles of interferon alpha and Beta in controlling Chikungunya virus replication and modulating Neutrophil-Mediated inflammation. *J Virol* **94** (2019).
68. Samuel, C. E. Antiviral actions of interferons. *Clin. Microbiol. Rev.* **14**, 778–809 (2001).
69. Xu, D. et al. Gr-1 + Cells other than Ly6G + Neutrophils limit virus replication and promote myocardial inflammation and fibrosis following coxsackievirus B3 infection of mice. *Front. Cell. Infect. Microbiol.* **8**, 157 (2018).
70. Dinarello, C. A. Immunological and inflammatory functions of the interleukin-1 family. *Annu. Rev. Immunol.* **27**, 519–550 (2009).
71. Smilde, B. J. et al. Colchicine aggravates coxsackievirus B3 infection in mice. *Int. J. Cardiol.* **216**, 58–65 (2016).
72. Afanasyeva, M. et al. Quantitative analysis of myocardial inflammation by flow cytometry in murine autoimmune myocarditis: correlation with cardiac function. *Am. J. Pathol.* **164**, 807–815 (2004).
73. Frangogiannis, N. G. Cardiac fibrosis. *Cardiovascular. Res.* **117**, 1450–1488 (2021).
74. Bai, F. et al. IL-10 signaling Blockade controls murine West nile virus infection. *PLoS Pathog.* **5**, e1000610 (2009).
75. Bai, F. et al. Use of RNA interference to prevent lethal murine West nile virus infection. *J. Infect. Dis.* **191**, 1148–1154 (2005).
76. Bai, F. et al. A Paradoxical role for neutrophils in the pathogenesis of West nile virus. *J. Infect. Dis.* **202**, 1804–1812 (2010).
77. Paul, A. M. et al. Osteopontin facilitates West nile virus neuroinvasion via neutrophil Trojan horse transport. *Sci. Rep.* **7**, 4722 (2017).
78. Nazneen, F. et al. An effective live-attenuated Zika vaccine candidate with a modified 5' untranslated region. *NPJ Vaccines*. **8**, 50 (2023).
79. Chintapula, U. et al. A novel nanocomposite drug delivery system for SARS-CoV-2 infections. *Nanoscale Adv.* **6**, 3747–3758 (2024).
80. Wiggins, J. et al. Identification of a novel antiviral lectin against SARS-CoV-2 Omicron variant from Shiitake-Mushroom-Derived Vesicle-like nanoparticles. *Viruses* **16** (2024).
81. Yee, K. T. & Vetter, D. E. Detection of West nile virus envelope protein in brain tissue with an immunohistochemical assay. *Methods Mol. Biol.* **2585**, 51–69 (2023).
82. Archila, E. D., Lopez, L. S., Castellanos, J. E. & Calvo, E. P. Molecular and biological characterization of an Asian-American isolate of Chikungunya virus. *PLoS One*. **17**, e0266450 (2022).
83. Wang, Q. et al. Neuraminidase 1 exacerbating aortic dissection by governing a Pro-Inflammatory program in macrophages. *Front. Cardiovasc. Med.* **8**, 788645 (2021).

Acknowledgements

The authors thank Dr. Robert B. Tesh (University of Texas Medical Branch) for providing CHIKV strain LR OPY1 2006. The authors also thank the Mississippi INBRE (funded by the National Institute of General Medical Sciences GM103476) for use of the research facility.

Author contributions

F.B. conceived the experiments; S.U.K. conducted the experiments; F.Z., P.M.D. D., and D.S.B assisted in the experiments; D.R. provided experimental materials; F.B. and S.U.K. wrote the manuscript. All authors read and approved the manuscript.

Declarations

Competing interests

The authors declare no competing interests.

Additional information

Correspondence and requests for materials should be addressed to F.B.

Reprints and permissions information is available at www.nature.com/reprints.

Publisher's note Springer Nature remains neutral with regard to jurisdictional claims in published maps and institutional affiliations.

Open Access This article is licensed under a Creative Commons Attribution-NonCommercial-NoDerivatives 4.0 International License, which permits any non-commercial use, sharing, distribution and reproduction in any medium or format, as long as you give appropriate credit to the original author(s) and the source, provide a link to the Creative Commons licence, and indicate if you modified the licensed material. You do not have permission under this licence to share adapted material derived from this article or parts of it. The images or other third party material in this article are included in the article's Creative Commons licence, unless indicated otherwise in a credit line to the material. If material is not included in the article's Creative Commons licence and your intended use is not permitted by statutory regulation or exceeds the permitted use, you will need to obtain permission directly from the copyright holder. To view a copy of this licence, visit http://creativecommons.org/licenses/by-nc-nd/4.0/.

© The Author(s) 2025